Imbricated slip rate processes during slow slip transients imaged by low-frequency earthquakes

O. Lengliné [a,*], W.B. Frank [b], D. Marsan [c], J.-P. Ampuero [d]

[a] *Université de Strasbourg, EOST, IPGS, CNRS, Strasbourg, France*
[b] *Department of Earth, Atmospheric, and Planetary Sciences, MIT, Cambridge, USA*
[c] *Université de Savoie, IsTerre, CNRS, Le Bourget du Lac, France*
[d] *Seismological Laboratory, California Institute of Technology, Pasadena, USA*

A B S T R A C T

Low Frequency Earthquakes (LFEs) often occur in conjunction with transient strain episodes, or Slow Slip Events (SSEs), in subduction zones. Their focal mechanism and location consistent with shear failure on the plate interface argue for a model where LFEs are discrete dynamic ruptures in an otherwise slowly slipping interface. SSEs are mostly observed by surface geodetic instruments with limited resolution and it is likely that only the largest ones are detected. The time synchronization of LFEs and SSEs suggests that we could use the recorded LFEs to constrain the evolution of SSEs, and notably of the geodetically-undetected small ones. However, inferring slow slip rate from the temporal evolution of LFE activity is complicated by the strong temporal clustering of LFEs. Here we apply dedicated statistical tools to retrieve the temporal evolution of SSE slip rates from the time history of LFE occurrences in two subduction zones, Mexico and Cascadia, and in the deep portion of the San Andreas fault at Parkfield. We find temporal characteristics of LFEs that are similar across these three different regions. The longer term episodic slip transients present in these datasets show a slip rate decay with time after the passage of the SSE front possibly as $t^{-1/4}$. They are composed of multiple short term transients with steeper slip rate decay as $t^{-\alpha}$ with α between 1.4 and 2. We also find that the maximum slip rate of SSEs has a continuous distribution. Our results indicate that creeping faults host intermittent deformation at various scales resulting from the imbricated occurrence of numerous slow slip events of various amplitudes.

© 2017 Elsevier B.V. All rights reserved.

1. Introduction

Faults are complex interfaces with heterogeneous properties. This is notably reflected by the large fluctuations of fault surface topography found over a broad range of scales on fault outcrops (Candela et al., 2009). Deciphering the physics of fault systems is challenging due to the wide range of time and spatial scales associated with fault slip (Ben-Zion, 2008). Our ability to probe the dynamics of fault systems at depth is limited by the coarse spatial resolution provided by surface data (e.g. Radiguet et al., 2011). A common conceptual framework to rationalize the diversity of fault slip behavior is a model of fault interface consisting of locked, unstable patches capable of nucleating earthquakes and embedded in a stable fault matrix capable of steady or transient aseismic slip. The interactions between these two rheological components lead to a rich variety of phenomena such as slow slip events (SSEs) (e.g. Radiguet et al., 2011), earthquake swarms (e.g.

Lohman and McGuire, 2007; Villegas-Lanza et al., 2015), creep episodes recorded along strike slip faults (Wesson, 1988; Jolivet et al., 2015; Rousset et al., 2016) or in laboratory experiments (Måløy et al., 2006; Lengliné et al., 2012), afterslip (e.g. Miyazaki et al., 2004) and earthquake triggering mediated by elastic stress transfers (e.g. Dieterich, 1994) or by intervening aseismic slip transients (e.g. Ariyoshi et al., 2009, 2012; Lui and Lapusta, 2016). The main ingredients describing the dynamics of such interfaces are i) slow loading, ii) the heterogeneous nature of the medium and iii) long range elastic interactions. We can gain insight into the overall loading and stressing cycles of faults by analyzing the temporal behavior of slip in different geological contexts. Because direct imaging of small-amplitude slow slip at depth is often not possible, here we exploit the seismic signals that accompany slow slip, which we consider markers of the local slip rate on the fault interface (Frank, 2016). By analyzing such signals and their statistical properties we obtain information about the physics of the deforming heterogeneous medium and find that the transient deformation on different faults share common features, suggesting a common mechanical process.

Low frequency earthquakes (LFEs) are a particular type of seismic event recorded in several subduction zones and strike slip faults. They are characterized by a depletion in radiated energy at high frequencies compared to regular tectonic earthquakes. LFEs occur in environments where mostly aseismic slip is expected, generally in swarms forming tectonic tremors and often in conjunction with geodetically-detected slow slip transients. Numerous observations indicate that LFEs result from the dynamic shear failure on an otherwise aseismic interface (Shelly et al., 2006; Ide et al., 2007; Frank et al., 2013; Royer and Bostock, 2014). If LFEs can be considered a passive monitor of slow slip at depth (Shelly et al., 2011; Frank and Shapiro, 2014; Frank et al., 2015a,b), they provide high-resolution information about the spatio-temporal evolution of aseismic transients (Frank, 2016).

Indeed the concomitant increase of tremor/LFE activity and transient strain recorded by surface sensors suggests that both signals share the same mechanical origin. The propagation of a slow slip pulse along the fault interface is generally considered as both the driver of LFEs and the source of surface displacements associated with SSEs (Bartlow et al., 2011). Such slow slip fronts are also predicted by numerical and theoretical models of velocity-dependent frictional interfaces (Ariyoshi et al., 2009, 2012; Hawthorne and Rubin, 2013a). However the limited sensitivity and resolution of geodetic instruments severely challenges the detection of transient deformation episodes such that only the largest SSEs are captured. LFEs are detected all the time, yet SSEs are not. Most likely, weak transient deformation episodes have gone undetected. Notably, in the Parkfield segment of the San Andreas fault, numerous LFEs are recorded but no geodetic signals have been reported from deep slow slip events (Johnston et al., 2006). Here we propose to use LFEs to characterize the small amplitude transients invisible to GPS. Yet, the analysis of LFE activity is not straightforward and requires a detailed processing in order to relate the analyzed signal to the slip on the interface. This difficulty is especially related to the strong time-clustering of the LFE activity at short time-scale, which can dominate the signal (Trugman et al., 2015). We thus develop here a new method to extract the signature of slow slip events from the discrete occurrence of LFEs.

We analyze the timing of LFEs in order to constrain the temporal evolution of the process that drives them. We focus our analysis on LFEs identified in two subduction zones, Mexico and Cascadia, and on the deep portion of the San-Andreas fault at Parkfield. The activity of LFEs is often bursty, with a majority of events grouped into numerous short-lived swarms exhibiting high rates of LFEs (Frank et al., 2016). We first analyze the short-term dynamics of LFEs, revealing a strong clustering that decays quickly with time and that is present in all three datasets. These local short term transient episodes combine over longer time scales into bursts that we associate with SSEs. We show that such larger scale transient episodes occur all the time and with a variable amplitude. The decay of the event rate with time during these bursts illuminates the underlying slow slip rate, indicating a decay of both the slip velocity and the propagation speed of the SSE front with time.

2. LFE catalogs

All LFEs analyzed in this study have been detected through matched-filter searches based on their similarity to previously identified template waveforms (Gibbons and Ringdal, 2006). The LFEs associated with a common template will be referred to as a family. The high similarity of waveforms among LFEs of a given family indicates they originate from very closely located sources. Based on the current location methods, we cannot distinguish if a family is generated by a single source or by distinct sources distributed in a compact area. Here we consider each family represents the repetitive failure of the same asperity along the fault
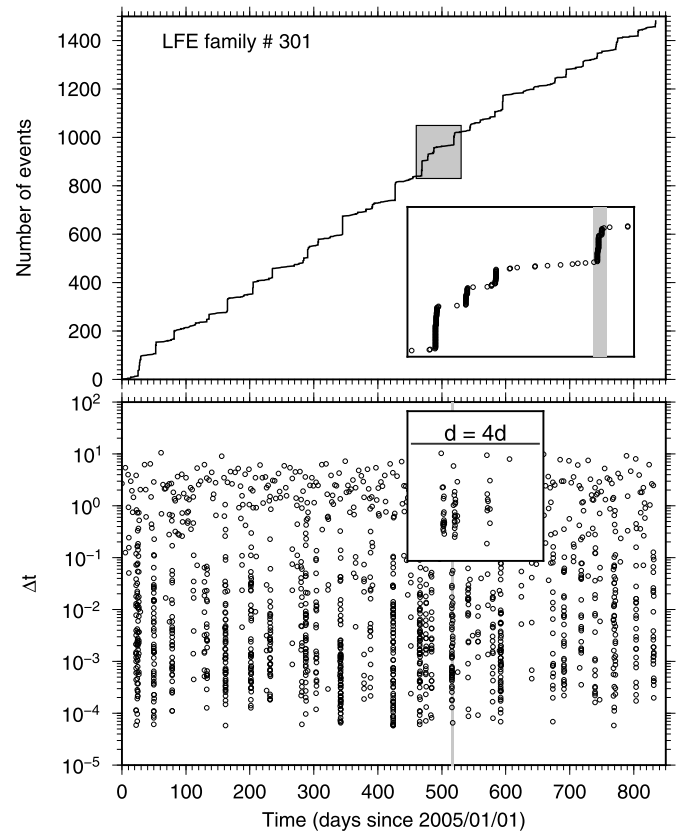
Fig. 1. Example of an LFE family detected on the Mexican interface. Top: The cumulative number of events in the family is displayed as a function of time. We observe an intermittent activity with bursts of LFEs making up the majority of events. The inset shows a zoom of the time period indicated by the gray box. Bottom: LFE recurrence times as a function of time. Bursts appear as vertical streaks of symbols. The inset shows a zoom of the time period indicated by the 4-day long gray interval in the inset of the top figure. We observe that the burst itself is composed of a succession of very short term sequences.

plane. We latter support this assumption based on our modeling results.

The LFE activity appears time clustered, with a majority of the LFEs in a family occurring during several bursts with only a few events in between (Frank et al., 2016) (Fig. 1).

We use three LFE catalogs in this study (Table 1). We first use a catalog of LFEs that occurred between January 2005 and April 2007 in the Mexican subduction zone (Frank et al., 2014). Some of the LFE families nearest to the trench are perturbed by the occurrence of a large slow slip in 2006 (Radiguet et al., 2011). We also analyze events in the Cascadia subduction zone, underneath Vancouver Island, from the catalog reported in Bostock et al. (2012). The LFEs in this catalog are only reported during the occurrence of large SSEs across almost 11 years, from February 2003 to October 2013. We use as well the Parkfield LFE catalog which comprises 88 LFE families that occurred on the deep portion of the San Andreas fault (Shelly and Hardebeck, 2010; Shelly, 2017). Events in this catalog are distributed over a 10 year long period extending from April 2001 to January 2010, but we only consider LFEs that took place after July 2005, in order to mitigate the impact of the September 2004, M_w6 earthquake on our analysis.

3. Model

We propose a statistical model that aims to reproduce the observed rate of LFEs as a function of time in a given family. No spatial dependence is taken into account in our model and we do not consider any explicit interaction between families. This does

Table 1

Analyzed catalogs of LFEs. Note that the Cascadia catalog only covers events during slow slip (Bostock et al., 2012).

Region	Total LFE count	# of LFE families	Average family count	Median family count
Mexico	1,849,487	1120	1651	853
Northern Cascadia	269,586	130	2073	1945
Parkfield	428,268	88	4867	4166

not necessarily imply an absence of space–time correlation of LFE rates between the different families. Indeed we observe some clear patterns indicating such correlation. However we do not try to model this interaction. This would add extra complexity to the analysis of the LFE rate and requires a dedicated model for rendering this spatial interaction. We rather decide to treat each family independently.

We assume in our model that the occurrence of LFEs is driven by an unknown external process. As we consider LFEs as repeaters, the most simple interpretation of this external process is slip on the fault area that surrounds the LFE-generating asperity. We are interested in recovering the temporal properties of this external process by studying its influence on the LFE activity rate. We note the LFE rate in a given family at a time t,

$$\lambda(t) = \mu + \sum_{i|t_i<t}^{Ne} a_i g(t - t_i),\tag{1}$$

where μ is the background LFE rate and the second term corresponds to the activation of LFEs by all preceding external processes (slip rate increase in our interpretation). This second term is composed of the amplitude a_i, which corresponds to the total number of LFEs induced by the i-th transient slip rate increase, and the normalized kernel, g, which is time-dependent and assumed the same for all SSEs in a given family. We note t_i the onset time of the i-th transient. We impose an *a priori* on the possible transient onset times by simply considering all the LFE times as a potential time (that is, the t_i are given by the time of LFEs in a family). If the LFE rate does indeed reflect loading velocity fluctuations, then using the LFE times as an *a priori* sampling of the possible transient onset times is a natural choice.

The number of LFEs in the family is denoted by N_e. We make no assumption on the shape of $g(t)$ and simply use a piecewise constant discretization of the kernel:

$$g_k = g(T_k < t < T_{k+1}),\tag{2}$$

where T_k are the time intervals used for discretization and $k \in [1 : N]$, with $T_1 = 0$ and $T_N = 10$ days. The kernel g is normalized such that it represents a probability density function (pdf),

$$\sum_{k=1}^{N} g_k(T_{k+1} - T_k) = 1.\tag{3}$$

We thus seek to recover the parameters μ, a_i and g_k that govern the LFE rate at any given time. We employ an Expectation-Maximization (EM) approach (Marsan and Lengliné, 2008, 2010; Veen and Schoenberg, 2008). The Expectation step is obtained by computing

$$\omega_{ij} = \frac{a_i g(t_j - t_i)}{\lambda(t_j)},\tag{4}$$

which corresponds to the probability that the LFE j is induced by a transient slip event starting at time t_i, and

$$\omega_{0j} = \frac{\mu}{\lambda(t_j)},\tag{5}$$

which is the probability that the LFE j is not induced by any previous transient episode. It implies that

$$\sum_{i=1}^{j-1} \omega_{ij} + \omega_{0j} = 1.\tag{6}$$

The cost function associated with Eq. (1) is thus

$$J = \mu T_m + \sum_{i=1}^{Ne} a_i G_i - \sum_{j=1}^{Ne} \omega_{0j} \ln(\mu)$$
$$- \sum_{j=1}^{Ne} \sum_{i<j} \omega_{ij} \ln\left[a_i g(t_j - t_i)\right]\tag{7}$$

where $G_i = \sum_{k=1}^{N} g_k \Delta_{ik}$ with $\Delta_{ik} = [T_k, T_{k+1}] \cap [0, T_m - t_i]$ and T_m is the duration of the time-series. For most events, $G_i = 1$ but because of the finiteness of the time series $G_i < 1$ for the last events of a family. The minimization step is then realized by finding the minimum of the cost function J, that is, canceling the partial derivatives of Eq. (7) with respect to the parameters of the problem:

$$\frac{\partial J}{\partial \mu} = 0 = T_m - \sum_{j=1}^{Ne} \frac{\omega_{0j}}{\mu}$$
$$\mu = \frac{\sum_{j=1}^{Ne} \omega_{0j}}{T_m},\tag{8}$$

$$\frac{\partial J}{\partial a_i} = 0 = G_i - \sum_{j>i}^{Ne} \frac{\omega_{ij}}{a_i}$$
$$a_i = \frac{\sum_{j>i}^{Ne} \omega_{ij}}{G_i},\tag{9}$$

$$\frac{\partial J}{\partial g_k} = 0 = \sum_{i}^{Ne} a_i \Delta_{ik} - \sum_{j=1}^{Ne} \sum_{i|T_k<t_j-t_i\leq T_{k+1}} \frac{\omega_{ij}}{g_k}$$
$$g_k = \sum_{j=1}^{Ne} \sum_{i|T_k<t_j-t_i\leq T_{k+1}} \frac{\omega_{ij}}{\sum_{i}^{Ne} a_i \Delta_{ik}}.\tag{10}$$

Once the parameters are estimated we iterate to another Expectation step, Eqs. (4)–(5), and Maximization step, Eqs. (8)–(10). We stop when the variation of the background rate, μ, between two successive iterations becomes smaller than a certain tolerance. In such a way, we constrain the background rate μ, the amplitude a_i associated with each time t_i, and the influence kernel g_k.

4. Short time-scale dynamics

4.1. Temporal evolution

We first apply this method to each LFE family in the Mexican LFE catalog. We recover the kernel $g(t)$, which captures the main time correlation among the events of a family and indicates a very short time clustering as visible in Fig. 1. We observe that $g(t)$ decays with time for all families (Fig. 2). This decay can be well approximated by a power-law function up to almost 1 day for

most of the families. We fit the power law decay of g and note p the power law exponent of the best fitting model for each family. The fit is performed in the range $t \in [10^{-3} - 0.3]$d. At lower time-scales, the onset of the power-law is not always well defined and at longer time scales (when the rate is the lowest), the convergence of the model is the most uncertain and may depend on the initial values of g. We obtain p values distributed between 0.5 and 2.0; the mean of the distribution is 1.3.

For the Cascadia catalog we find a similar power-law decay of the kernel with time. The best power-law fit yields an exponent p between 1.0 and 1.5, with a mean value of 1.3 (Fig. 2). For the Parkfield LFE catalog, $g(t)$ displays a rather different behavior compared to the two other catalogs. We still observe a power-law decay of g at short time-scales but this decay stops after approximately 0.01 days (15 minutes). Then, depending on the family, we find that either this rate stays at a constant value up to the longest time-scales or that the decay resumed after some longer time scale. We fit the power-law decay of g but restrict the time range for fitting to $[3 \cdot 10^{-4} - 10^{-2}]$d. The values of p that we obtain are significantly larger than the ones found for the two other study regions: the majority of p values range between 1.5 and 2.5 with a mean of 2.0.

The time clustering of the LFE activity shows a rapidly, power-law decaying rate, with region-dependent power-law exponent. In Parkfield, the time clustering is pronounced and the kernel g decays sharply. This reveals that our model mostly captures the short time-scale dynamics ($<$1d) of the LFE activity. We observe an agreement between the distribution of normalized recurrence times and the temporal decay of g, which supports the ability of our EM algorithm to correctly explain the data (Supplementary Figs. S1 and S2).

4.2. An external process

The power law decay of the kernel is very similar to the evolution of earthquake aftershock sequences. Omori's law describes how earthquake rates following previous earthquakes decay as a power law function of time. In earthquake-mainshock sequences, the emergence of Omori's law is mainly interpreted as being caused by the stress redistribution within the crust caused by the mainshock and by subsequent aftershock interactions.

Empirically, the larger the mainshock, the higher the number of triggered earthquakes. In the case of LFEs, the emergence of a power-law decay of the LFE rate at short time scales could have two main interpretations: i) the decay reflects the local triggering of LFEs by a preceding LFE, possibly by static stress changes similar to normal earthquake mainshock-aftershock sequences, or ii) the decay is rather a manifestation of an external process affecting the LFE rate, typically the loading rate imposed by an ongoing slip transient. In order to test these two scenarios, we check if the amplitudes of the LFEs are linked to the value of a_i, which corresponds to the number of induced events for a process starting at time t_i. Indeed one could expect that if LFEs are triggering other LFEs, the highest amplitude LFE (reflecting a larger event) would trigger a larger number of events and have a correspondingly high value of a. We hypothesize that the stress perturbation caused by an LFE is small enough such that its influence extends only to the family it belongs to but does not reach other families. For all the families in all three catalogs, we tested if there is any correlation between the amplitude of the LFE and the obtained values of a. In each case we find that this correlation is nearly absent (see Supplementary Fig. S3). This observation suggests that the time clustering of the LFE activity is not related to the amplitude of the initial LFE (within the same family). We also observed that the LFE amplitudes are marginally variable, so if triggering by LFE existed, then the rate of LFEs should be more or less constant, rather than the
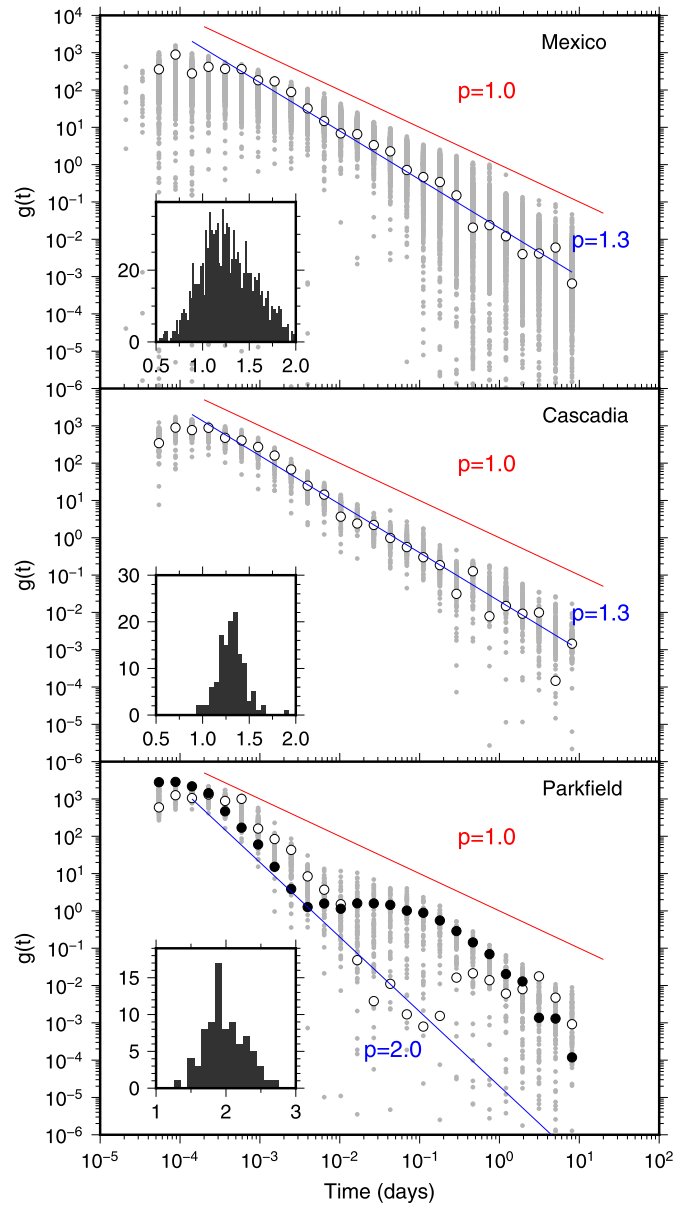

Fig. 2. Representation of all kernels (gray dots), g as a function of time for all families in the three LFE catalogs. The white circles show an example of the kernel g for a single family from each catalog. In the case of Parkfield, two examples are displayed (white and black circles) to illustrate the variability of the kernel among families. For each plot, the histogram represents the exponent of the best power-law fit of each kernel.

intermittent burst-like time series that are observed. This shows that the increase of the LFE rate is not caused by the occurrence of a preceding LFE but is rather the manifestation of an external process. It also confirms a posteriori our hypothesis that events in a family are produced by the same source. Indeed, if LFEs were very close but distinct asperities we would expect these asperities to interact and trigger each other. Our observation that, for some LFEs, a is nearly 0 and does not depend on the LFE amplitude does not support such interactions, but rather the interpretation that LFEs of a common family are repeating failures of the same fault patch.

4.3. Amplitude of the short transient episodes

The estimation of the coefficient a_i gives us insight into the number of events induced by a process initiating at time t_i. We observe that within a family, a large proportion of the amplitudes
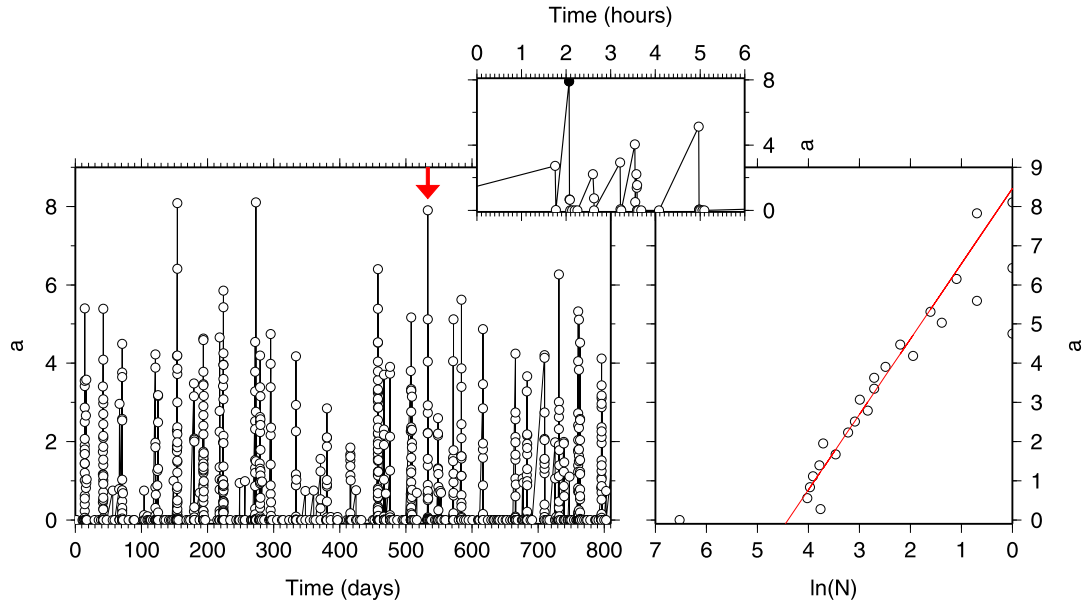
Fig. 3. Left: amplitude coefficients, a_i, as a function of time for a family of the Mexican LFE catalog. The red arrow indicates the time period around a burst shown in the middle panel. Middle: Same as the left figure with the time window centered on a burst of LFEs. The black circle represents the onset of the burst episode as defined in Section 5. Right: distribution of the coefficients a_i for the example represented on the left. The red line shows the best exponential fit of the distribution excluding the first interval comprising almost zero amplitude. (For interpretation of the references to color in this figure legend, the reader is referred to the web version of this article.)
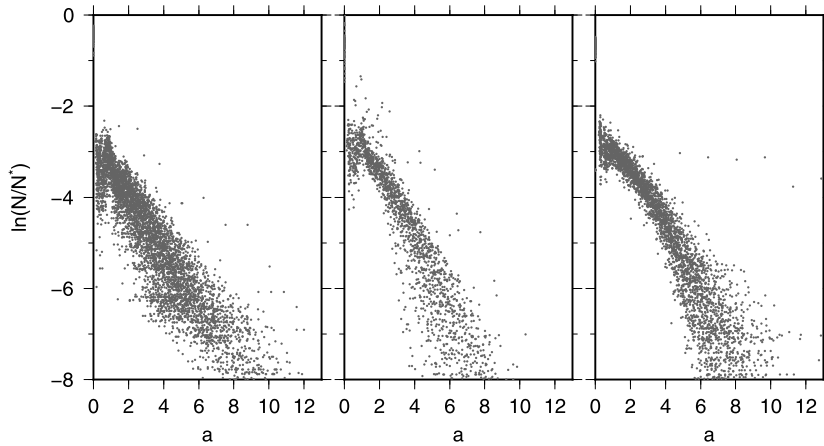
Fig. 4. Distribution of the transient episode amplitudes a (gray dots), with $a > 0$, for all families and for the three catalogs (from left to right: Mexico, Cascadia and Parkfield).

a are close to 0 (Fig. 3). This reflects the fact that many of the considered possible times of SSE actually do not correspond to any SSE onset.

We also observe that during a LFE burst several large values of a are present and not just a single large value of a at the onset of the burst (Fig. 3). This suggests that burst episodes are composed of a superposition of short time-scale sequences decaying rapidly with time (following the shape of g). We look at the distribution of the amplitudes a within a given family after excluding the low values of $a \simeq 0$ that do not represent a loading process. We observe for all families and all LFE catalogs that the distribution of the amplitude a can be well fitted by an exponential distribution h of the form

$$h(a) \propto \exp\left(-\frac{a}{a^*}\right) \tag{11}$$

where a^* is a fitting parameter (see Fig. 4). We find that the values of a^* are very narrowly distributed and are close to 2.0 for all families and for all catalogs. This exponential amplitude dependence, suggests that during a burst episode a hierarchy of transient slip rate processes are activated, all decaying with the same pattern in time but with variable amplitudes.

5. Long transient slip rate decay

So far, we have modeled the LFE time series without knowledge of the possible, long timescale transient episodes (SSE) occurrence times. Our model results mostly reflect the short-time scale dynamics of the LFE rate fluctuations imposed by a rapidly decaying slip rate process. We will now attempt to capture SSEs corresponding to burst periods of LFEs and that represent a longer time scale process as compared to the short decay of $g(t)$. The signature of this process his hidden by the strong time clustering imposed by g on the LFE rate, such that this influence has to be removed in order to extract the sole response of the SSE transient. We are first interested in recovering the temporal shape of the global process that affects the occurrence rate of LFEs during bursts. We use the parameters a and ω_0 to isolate events that mark the onset of a burst episode.

We identify the onset of burst periods as possible times where i) the transient forcing amplitude, a, is distinct from 0, because we are interested in periods of enhanced activity, and ii) the value of ω_0 is significantly different from 0, because we want to capture only the onset of the burst i.e. there exists a sufficiently large tem-

poral gap with the preceding event. We note that imposing such a criterion, we may miss the exact onset time of the burst episode if the related LFE rate activity is emerging slowly from background and not sharply.

Consequently, for each family, we define the start of a burst as time t_i for which $a_i/a_{max} > a_c$ and $\omega_0 > \omega_{0c}$, where a_{max} is the maximum value of a_i for a given family and a_c is a threshold fixed at 10^{-2}. We define the threshold ω_{0c} as the minimum of the ω_0 distribution, which marks the transition between the induced and background populations. We check that increasing this threshold or changing the value of a_c do not affect significantly our results (see Supplementary Figs. S4–S5). We also hypothesize that two SSEs cannot occur at the same time on a given family and we impose that in a family there could be only one burst episode in a time period less than $4\langle \Delta t \rangle$, where $\langle \Delta t \rangle$ is the mean inter-LFE time. If we find more than one possible burst onset time in such a time period we only keep the time associated with the highest value of a.

Once burst onsets have been isolated with the criterion presented above, we simply compute the rate of induced LFEs following the burst onset in order to retrieve the mean evolution of the external process affecting the family (C). For all families we compute C as:

$$C(t, t + \delta t) = \frac{1}{N_b} \frac{1}{\delta t} \sum_{n=1}^{Nb} \sum_{j|t_j > t_n} (1 - \omega_{0j}) \Theta(t < t_j - t_n < t + \delta t),$$
(12)

where N_b is the number of bursts in a given family, and the times t_n are the burst onset times. The function $\Theta(P) = 1$ if the proposition P is true and equals 0 otherwise. We then separately stack the functions C for all families of a given catalog. By this procedure we can only recover aspects of the temporal evolution of the SSE that are common to all bursts and families. If each SSE has a different slip velocity shape, we might loose this information when averaging. For all catalogs we observe a very slow decay of C at early times (Fig. 5). This decay then transitions to a new rate which finally merges with the LFE rate that precedes the burst and defines the end of the burst period. In the Cascadia catalog, because no LFEs are reported outside burst periods (here identified as the large SSE), $C(t)$ decays to 0 at long time scale instead of flattening to the background rate. For the Mexican and the Cascadia catalogs we observe that the slow decay of C, before the sharp decay indicating the end of the burst period, can be well approximated by a power-law decay function with an exponent of 0.25 (Fig. 5). In the Parkfield catalog, we observe that the function C decays quickly between 10^{-3}d and 10^{-1}d and then more slowly decays before reaching the background rate at around 2 to 10 days. We also observe in Fig. 5 that the kernel, g, associated with each catalog decays much more quickly than $C(t)$ indicating that bursts must comprise multiple fast transient sequences as already speculated.

6. Burst recurrence times

We now turn to the recurrence times of the SSE. We consider the onset times that we obtained in the previous section. For each family we compute the inter-burst times and normalize them by the mean inter-burst time of the family. We only consider families from all catalogs that have at least 5 bursts occurrences. We then merge all computed values for each families in order to obtain a single distribution of normalized recurrence times for each catalog (Fig. 6).

We observe that the pdfs of the normalized burst recurrence times exhibit a maximum around $\Delta T_B / \overline{\Delta T_B} \sim 1$, where ΔT_B is the burst recurrence time. The pdfs then decay sharply away from
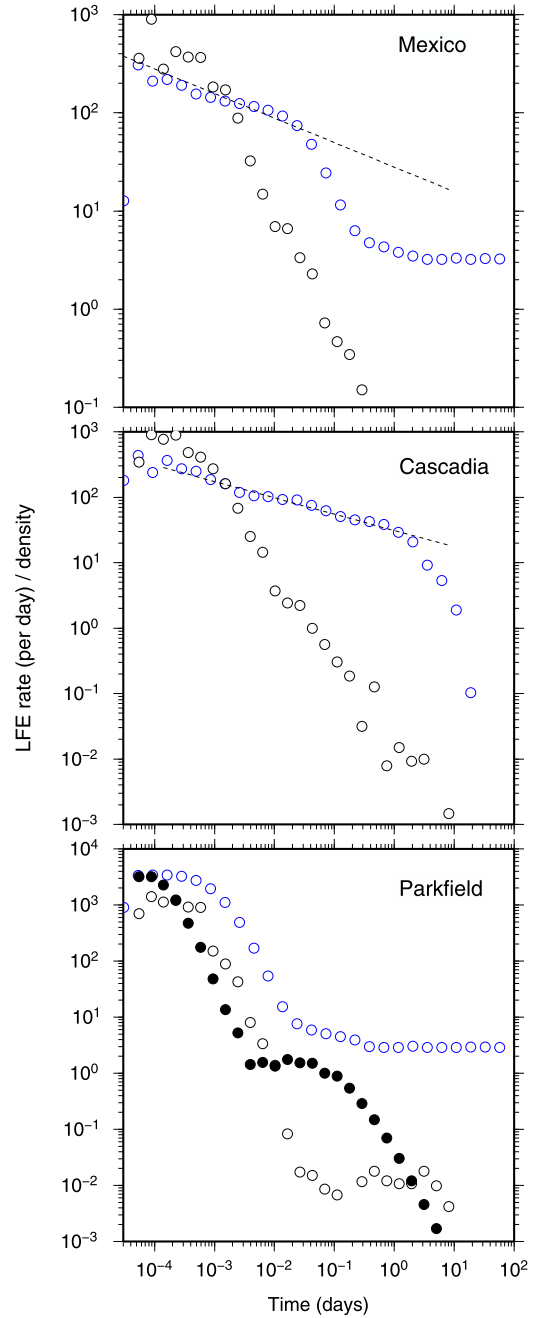

Fig. 5. Evolution of the function $C(t)$ (blue circles) for the three catalogs. The dashed lines show a power-law decay function with an exponent of 0.25. We also represent, for each catalog, examples of the kernel, $g(t)$, (white and black circles) that are presented in Fig. 2. (For interpretation of the references to color in this figure legend, the reader is referred to the web version of this article.)

this maximum. The shape of the pdfs describing these recurrence times is well approximated by a log-normal distribution (Fig. 6).

Although we try to define as objectively as possible the burst timing, this step relies on *ad hoc* thresholds. In order to check the validity of our approach, we compare our results with other results obtained using a different approach to extract burst occurrence times. We follow the approach presented in Wu et al. (2015) and found that the burst recurrence times obtained with this method are compatible with the distributions obtained previously (Fig. S6). These results confirmed those obtained previously and show that the recurrence times over the interface are well approximated by a log-normal distribution. We also verify that, when a sufficient number of bursts are available in a given family, the individual pdf
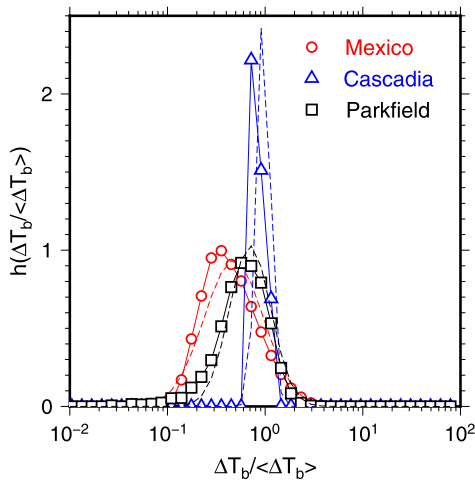
Fig. 6. Probability density functions of the normalized inter-burst times for the three catalogs (symbols and plain lines). The dashed lines show the best log-normal distribution fit to the data for the three catalogs.

computed for that family has a similar shape to the average pdf in Fig. 6. We conclude that the obtained distribution is not an artifact of the collective merging of families and is also valid at the scale of a single family.

7. Burst amplitude distribution

In order to appraise the amplitude of each burst we compute the number of non-background events during each burst period for a given family. Assuming that these LFEs represent repeating events, this amplitude can be considered as a proxy for the slip that occurred during the burst. We then normalize this number of events by the total number of events in the family. We merge all results from all the families of a common catalog in order to obtain the distribution of the burst amplitudes. We observe in Fig. 7 that this distribution is well fit by an exponential distribution for Mexico and Cascadia and by a power-law distribution for Parkfield. This suggests that the bursts as well have a variable amplitude and do not recur always with the same amplitude. We note that such variable amplitude was also inferred from the analysis of tremor although with a different amplitude distribution function (Wech et al., 2010).

8. Modeling the LFE activity

In order to appraise the validity of the presented model of LFE (Eq. (1)) we perform direct simulations of LFE time-series. We aimed at reproducing the observed statistical features of the LFE activity while generating LFEs according to Eq. (1). It also helps validate if Eq. (1) does represent a correct description of the LFE activity.

In order to do so we first generate background LFEs whose occurrence times are obtained from an homogeneous Poisson process of rate μ. We could consider that these events are linked to the background loading rate of the plate interface. We then consider two simulation scenarios in order to reproduce the non background events. First we simply suppose that at each time of a background event a short time scale transient episode, as captured by g, is happening. In order to model this scenario, we draw a random value of the amplitude a_i that represents the number of induced events and we generate the times of these events based on the kernel g. In such a scenario we are closely following Eq. (1) but without considering the burst behavior of LFE that we evidenced with the function C. We observe that such simulations always produce too intense bursts and with a too low apparent

periodicity (Fig. S7). In a second scenario, we simply considered that LFEs are only generated by the longer time-scale burst (SSE) events. We first generate SSE onset times. In order to do this, we used the results of Fig. 6 which shows that burst are recurring following a log-normal pdf. From these burst onset times we construct a non-homogeneous Poisson process with the rate evolving as $C(t)$ and limited over the duration of the SSE episode. We associate each of these times with an LFE. In this scenario we are not respecting Eq. (1) and we observe that the resulting LFE time history is too regular and with no short-time activity (Fig. S7). Finally, we combine the two previous scenarios in order to produce simulations that both respect Eq. (1) but also consider the burst properties as evidenced by the burst recurrence times and the function C. In order to do this, we proceed as for the previous scenario but instead of considering that the function C is directly responsible for the LFEs, we now impose that the generated times represent the times of the short-time scale episodes that are responsible for the LFE activities. We finally generate LFEs by: first drawing random values of a in an exponential distribution (as implied from Fig. 4) at each times generated at the previous step, and then obtain the LFE times considering a non-homogeneous Poisson process of amplitude a and decaying following $g(t)$. Adding the background events to these induced LFE events we are thus obtaining LFE time-series that respect the model imposed by Eq. (1). The simulations produced with this last scenario are much more in agreement with the observed time history of LFEs (Fig. 8). This result can be compared with Fig. 1 which shows the actual family in the catalog.

This agreement is attested by the comparison of the value of J as defined by Eq. (7) computed for the family of the catalog and 100 random realizations of the time-series that have similar statistical features with the tested family. We observe that the value of J of the true sequence is of the same order of magnitude as the ones computed from our synthetic sequences (Fig. 8). We find that for 100 randomly selected families, the proportion γ as defined in the L-Test, as the proportion of generated models with a lower likelihood than the tested data, is $\gamma = 55\%$ (Schorlemmer et al., 2007). The observed likelihood is in the middle of the simulated values, suggesting that the proposed model is consistent with the data. It shows that our model is capturing most of the temporal dynamics of the LFE sequence. It also demonstrates *a posteriori* that the description of LFE activity as proposed by Eq. (1) is a valid model.

9. Discussion

We demonstrate that the dynamics of LFE activity in three different plate boundaries share many common properties. The LFEs occur mostly during bursts of high event rates that comprise several fast-decaying transient episodes.

During bursts, we show that the LFE activity is strongly time clustered at short time scales. Indeed, because bursts have a duration that is longer than a single short time-scale sequence (Fig. 5) and because we observe several large values of the amplitudes, a, during a single burst event, we suggest that burst sequences are composed of a succession of transient slow slip episodes.

Several hypotheses can be proposed to explain this short-time clustering of the local rapid episodes. We previously did not favor the possibility that LFEs are triggering other nearby LFEs, either by static stress transfer caused by slip on the LFE patch or by the associated post-seismic stress relaxation. We thus suggest that an external forcing (possibly an aseismic transient or SSE) is responsible for the LFE rate. If we hypothesize that the LFE rate is proportional to the loading rate in the creeping portion of the fault that undergoes a local creeping event, then the temporal decay of g represents a local instability on the fault over a short time
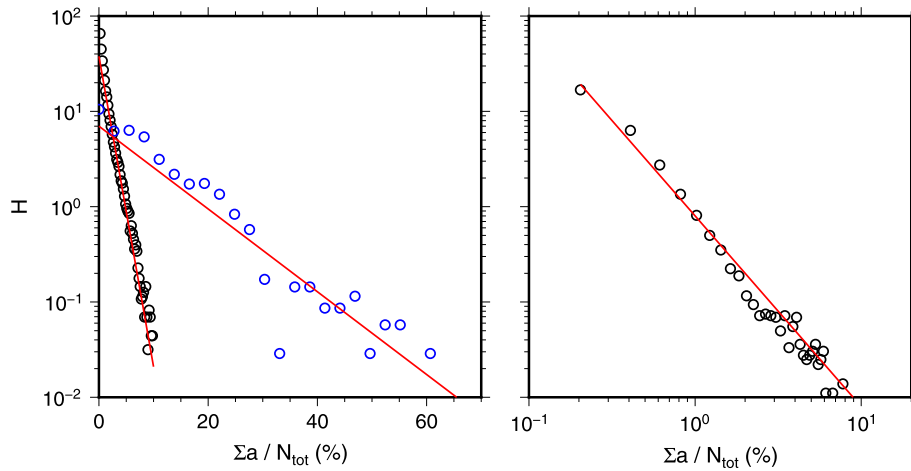
Fig. 7. Left: Probability density function, p of the normalized burst amplitude for the Mexican (black) and Cascadia (blue) catalogs. The red line shows the best exponential fit of the distribution. Right: Same distribution for the Parkfield catalog. (For interpretation of the references to color in this figure legend, the reader is referred to the web version of this article.)

scale. The time clustering of the LFE in a family therefore reflects an activation through a transient increase of the local loading rate. Following this scenario it requires that the loading rate during a SSE fluctuates rapidly at the location of the family because several fast decaying episodes are taking place during an SSE. In this case the LFE patch is activated multiple times during the burst period. This could be possible for instance if the macro-SSE pulse contains multiple mini-SSE pulses. Such a complex interweaving of variable time-scales and amplitude of transient slip episodes would be consistent with the very complex swarm patterns of tremor found in Mexico (Peng and Rubin, 2016). These could also be explained by invoking sub-events that develop as back-propagating fronts notably during rapid tremor reversals (Hawthorne and Rubin, 2013b). This is supported by geodetic observations revealing that back propagating sub-events may compose the overall slow slip event (Hawthorne et al., 2016). High precision location of LFE sources in Cascadia shows that most LFEs are related to these very short term transient episodes in secondary fronts that develop during larger scale SSEs (Rubin and Armbruster, 2013), as observed here. We can thus assume that the observed sharp decay of $g(t)$ reflects the modulation of the slip rate at a given location during these back-propagating fronts or also possibly during fast along-dip migration.

A second interpretation is that a LFE family actually comprises multiple nearby patches capable of nucleating LFEs. All these patches react to the loading rate imposed locally by the slow-slip event. The burst episodes we observe are then a combination of the time-varying slip rate at the location of a single LFE patch combined with the spatial extent of the slow slip front reaching other LFE asperities (possibly included in the same family). This implies that a mini-SSE can be large enough to cover multiple families. This could explain the space–time correlation observed for LFE in Mexico (Frank et al., 2016).

The evolution with time of the LFE activity within a burst when combining multiple sequences and/or families shows that the decay is very slow at the beginning of the burst, possibly decaying as a power-law with an exponent close to 0.25. This might be a true feature of the SSE indicating that the slipping rate is decaying slowly over the SSE duration at a given location of the passing SSE pulse. This could also reflect other possible scenarios. First, we might be missing the exact onset of the SSE/burst. This can effectively happen if the SSE onset is emergent and because we are sampling the possible onset times only at the time of LFEs. Another possibility is that because we are mixing several slow slip episodes with variable rise time and duration, we recover an aver-

age evolution that masks the true decay of the SSE velocity. If we interpret the slow decay of the LFE rate during bursts as the signature of the slip rate imposed by the passing SSE front, we can link our results with the SSE dynamics. Indeed, rate and state friction models indicate that the slip rate, v, behind the SSE front decays as a function of the distance from the front, d, as $v(d) \propto d^{-0.5}$ (Hawthorne and Rubin, 2013a). Our observation that $v(t) \propto t^{-0.25}$ then implies that $d(t) \propto t^{0.5}$. It suggests that the SSE front propagates with a decaying speed. The inferred migration pattern has been actually observed for LFEs in Japan, suggesting it might be a common feature of SSE (Ando et al., 2012). This indicates that our function C captures well the slip rate evolution of a burst at a given position of the fault plane. We can thus envision a model of variable fault slip rate over the plate interface governed mostly by two time-scale processes associated to the main SSE and the secondary transient fronts. The LFEs appear mostly during short term transient fronts whose occurrences are itself conditioned by a larger scale destabilization during an SSE (Fig. 9).

The numerous bursts/SSE episodes that we capture present a variable amplitude as quantified by the number of events occurring during these episodes (Fig. 7). If we interpret the number of events as the slip amplitude of each SSE, we find that SSE amplitudes are not constant but follow an exponential (Mexico, Cascadia) or power-law (Parkfield) distribution. This supports the idea that SSE captured by geodetic instruments at the surface only represent the larger, visible aseismic transients. Many other SSEs of smaller amplitudes are then missed because of the limited resolution of the surface instruments. Indeed, when seismological observations are leveraged to analyze the GPS time-series, evidence for previously unnoticed transient slip is recovered (Frank et al., 2015b; Frank, 2016). This argues in favor of the existence of SSEs of all sizes taking place over the fault plane as we observed from our analysis of LFEs and was observed from analysis of the tremor, although with a different amplitude distribution (Wech et al., 2010).

10. Conclusion

The analysis of the time history of LFEs reveals several common features across three different regions. We find evidence that the slip on the plate interface is dominated by a process with two time scales. At short time-scale we find an activity decreasing rapidly with time, possibly related to local transient episodes linked to rapid tremor reversals. We show that this activity at very short time scale is modulated by the occurrence of longer time-scale burst episodes related to slow slip events on the interface.
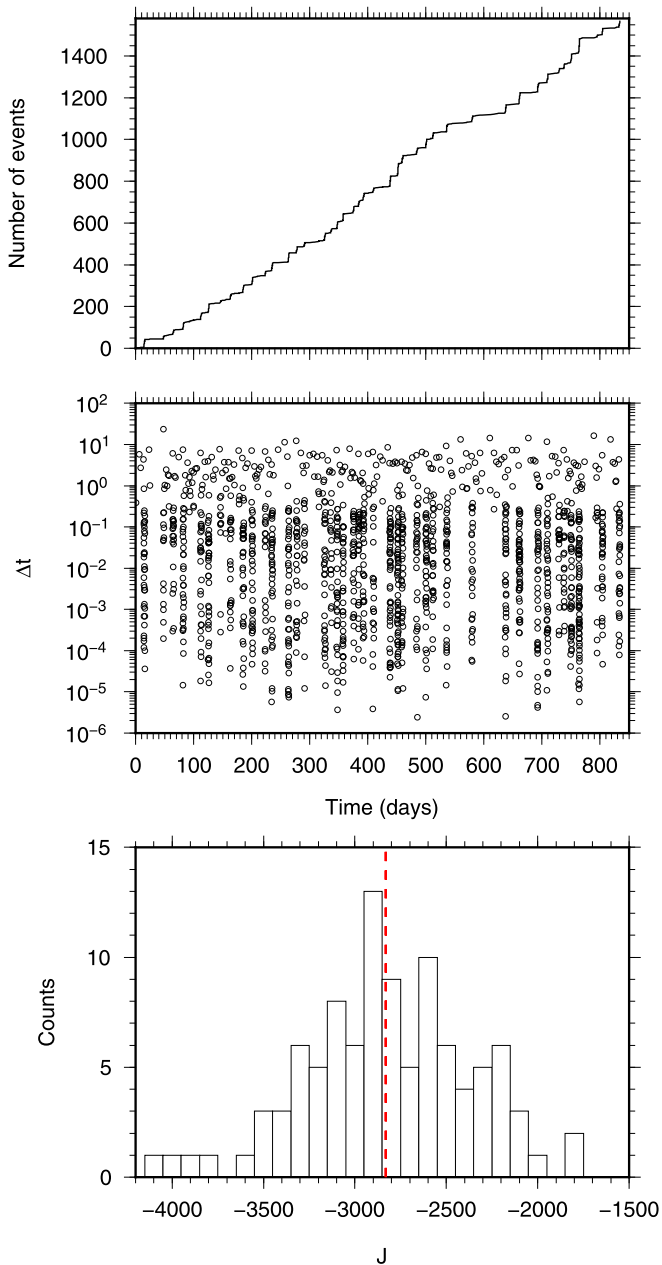
Fig. 8. Example of a random realization of a generated LFE family. This family was generated based on statistical properties of the family reported in Fig. 1. Top: cumulative number of LFEs in the family as a function of time. Middle: Recurrence time of LFE as a function of time. Bottom: Histogram of the value of J as defined by Eq. (7) computed for the 100 random realizations of this family. The red dashed line indicates the actual value of J computed for this family in the catalog. (For interpretation of the references to color in this figure legend, the reader is referred to the web version of this article.)

We show that the slip rate within a burst at a given location decays more slowly with time. The amplitude of these burst events follows a continuous distribution implying that SSEs of all sizes occur on the fault plane. These episodes can recur over a broad time interval. Our results suggest that the apparent, large-scale, continuous deformation of creeping faults is actually composed of a hierarchy of variable-amplitude slow slip events.

Acknowledgements

We thank D. Shelly and M. Bostock for providing access to their LFE catalog. We thank S. Yabe and an anonymous reviewer for their
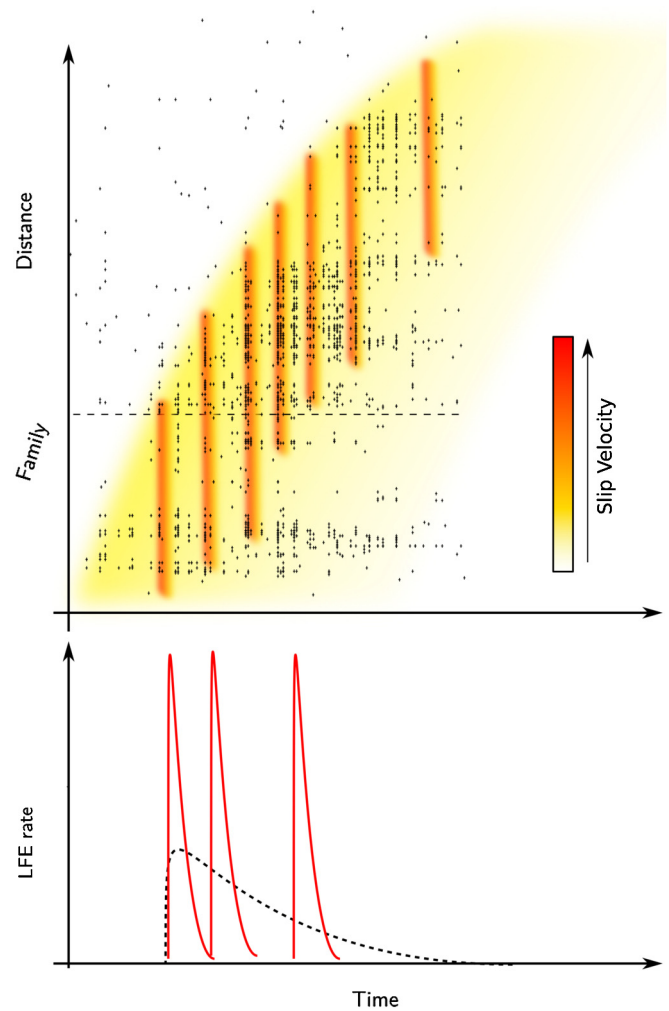
Fig. 9. Sketch illustrating LFE rate fluctuations in relation with the fault slip velocity. The colors represent the interface velocity in a time-space diagram. The black dots represent actual LFEs of the Mexican catalog extracted over a period of 12 hours and 15 km in the along dip direction. We observe an increase of the activity over the 12 hours that we link to the occurrence of an SSE. The slip rate of this SSE is represented by the black dashed curve at the bottom and corresponds to the function C. During this large scale transient multiple secondary fronts develop and activate LFEs over very short time scales (red colors). The very short time decay during these episodes is captured by the function g. (For interpretation of the references to color in this figure legend, the reader is referred to the web version of this article.)

Appendix A. Supplementary material

Supplementary material related to this article can be found online at http://dx.doi.org/10.1016/j.epsl.2017.07.032.

References

Ando, R., Takeda, N., Yamashita, T., 2012. Propagation dynamics of seismic and aseismic slip governed by fault heterogeneity and Newtonian rheology. J. Geophys. Res., Solid Earth 117.

Ariyoshi, K., Hori, T., Ampuero, J.-P., Kaneda, Y., Matsuzawa, T., Hino, R., Hasegawa, A., 2009. Influence of interaction between small asperities on various types of slow earthquakes in a 3-d simulation for a subduction plate boundary. Gondwana Res. 16, 534–544.

Ariyoshi, K., Matsuzawa, T., Ampuero, J.-P., Nakata, R., Hori, T., Kaneda, Y., Hino, R., Hasegawa, A., 2012. Migration process of very low-frequency events based on a chain-reaction model and its application to the detection of preseismic slip for megathrust earthquakes. Earth Planets Space 64, 693–702.

Bartlow, N.M., Miyazaki, S., Bradley, A.M., Segall, P., 2011. Space–time correlation of slip and tremor during the 2009 Cascadia slow slip event. Geophys. Res. Lett. 38.

Ben-Zion, Y., 2008. Collective behavior of earthquakes and faults: continuum-discrete transitions, progressive evolutionary changes, and different dynamic regimes. Rev. Geophys. 46.

Bostock, M., Royer, A., Hearn, E., Peacock, S., 2012. Low frequency earthquakes below southern Vancouver Island. Geochem. Geophys. Geosyst. 13.

Candela, T., Renard, F., Bouchon, M., Brouste, A., Marsan, D., Schmittbuhl, J., Voisin, C., 2009. Characterization of fault roughness at various scales: implications of three-dimensional high resolution topography measurements. Pure Appl. Geophys. 166, 1817–1851.

Dieterich, J., 1994. A constitutive law for rate of earthquake production and its application to earthquake clustering. J. Geophys. Res., Solid Earth 99, 2601–2618.

Frank, W.B., 2016. Slow slip hidden in the noise: the intermittence of tectonic release. Geophys. Res. Lett. 43.

Frank, W., Shapiro, N., 2014. Automatic detection of low-frequency earthquakes (lfes) based on a beamformed network response. Geophys. J. Int. 197, 1215–1223.

Frank, W.B., Shapiro, N.M., Kostoglodov, V., Husker, A.L., Campillo, M., Payero, J.S., Prieto, G.A., 2013. Low-frequency earthquakes in the Mexican sweet spot. Geophys. Res. Lett. 40, 2661–2666.

Frank, W.B., Shapiro, N.M., Husker, A.L., Kostoglodov, V., Romanenko, A., Campillo, M., 2014. Using systematically characterized low-frequency earthquakes as a fault probe in Guerrero, Mexico. J. Geophys. Res., Solid Earth 119, 7686–7700.

Frank, W.B., Radiguet, M., Rousset, B., Shapiro, N.M., Husker, A.L., Kostoglodov, V., Cotte, N., Campillo, M., 2015b. Uncovering the geodetic signature of silent slip through repeating earthquakes. Geophys. Res. Lett. 42, 2774–2779.

Frank, W., Shapiro, N., Husker, A., Kostoglodov, V., Bhat, H., Campillo, M., 2015a. Along-fault pore-pressure evolution during a slow-slip event in Guerrero, Mexico. Earth Planet. Sci. Lett. 413, 135–143.

Frank, W.B., Shapiro, N.M., Husker, A.L., Kostoglodov, V., Gusev, A.A., Campillo, M., 2016. The evolving interaction of low-frequency earthquakes during transient slip. Sci. Adv. 2, e1501616.

Gibbons, S.J., Ringdal, F., 2006. The detection of low magnitude seismic events using array-based waveform correlation. Geophys. J. Int. 165, 149–166.

Hawthorne, J., Rubin, A., 2013a. Laterally propagating slow slip events in a rate and state friction model with a velocity-weakening to velocity-strengthening transition. J. Geophys. Res., Solid Earth 118, 3785–3808.

Hawthorne, J., Rubin, A., 2013b. Short-time scale correlation between slow slip and tremor in Cascadia. J. Geophys. Res., Solid Earth 118, 1316–1329.

Hawthorne, J.C., Bostock, M.G., Royer, A.A., Thomas, A.M., 2016. Variations in slow slip moment rate associated with rapid tremor reversals in Cascadia. Geochem. Geophys. Geosyst..

Ide, S., Beroza, G.C., Shelly, D.R., Uchide, T., 2007. A scaling law for slow earthquakes. Nature 447, 76–79.

Johnston, M., Borcherdt, R., Linde, A., Gladwin, M., 2006. Continuous borehole strain and pore pressure in the near field of the 28 September 2004 m 6.0 Parkfield, California, earthquake: implications for nucleation, fault response, earthquake prediction, and tremor. Bull. Seismol. Soc. Am. 96, S56–S72.

Jolivet, R., Candela, T., Lasserre, C., Renard, F., Klinger, Y., Doin, M.-P., 2015. The burst-like behavior of aseismic slip on a rough fault: the creeping section of the Haiyuan fault, China. Bull. Seismol. Soc. Am. 105, 480–488.

Lengliné, O., Elkhoury, J., Daniel, G., Schmittbuhl, J., Toussaint, R., Ampuero, J.-P., Bouchon, M., 2012. Interplay of seismic and aseismic deformations during earthquake swarms: an experimental approach. Earth Planet. Sci. Lett. 331, 215–223.

Lohman, R.B., McGuire, J.J., 2007. Earthquake swarms driven by aseismic creep in the salton trough, California. J. Geophys. Res., Solid Earth 112.

Lui, S.K., Lapusta, N., 2016. Repeating microearthquake sequences interact predominantly through postseismic slip. Nat. Commun. 7, 13020.

Måløy, K.J., Santucci, S., Schmittbuhl, J., Toussaint, R., 2006. Local waiting time fluctuations along a randomly pinned crack front. Phys. Rev. Lett. 96, 045501.

Marsan, D., Lengliné, O., 2008. Extending earthquakes' reach through cascading. Science 319, 1076–1079.

Marsan, D., Lengliné, O., 2010. A new estimation of the decay of aftershock density with distance to the mainshock. J. Geophys. Res., Solid Earth 115.

Miyazaki, S.-i., Segall, P., Fukuda, J., Kato, T., 2004. Space time distribution of afterslip following the 2003 Tokachi-Oki earthquake: implications for variations in fault zone frictional properties. Geophys. Res. Lett. 31.

Peng, Y., Rubin, A.M., 2016. Intermittent tremor migrations beneath Guerrero, Mexico and implications for fault healing within the slow slip zone. Geophys. Res. Lett..

Radiguet, M., Cotton, F., Vergnolle, M., Campillo, M., Valette, B., Kostoglodov, V., Cotte, N., 2011. Spatial and temporal evolution of a long term slow slip event: the 2006 Guerrero slow slip event. Geophys. J. Int. 184, 816–828.

Rousset, B., Jolivet, R., Simons, M., Lasserre, C., Riel, B., Milillo, P., Çakir, Z., Renard, F., 2016. An aseismic slip transient on the North Anatolian fault. Geophys. Res. Lett. 43, 3254–3262.

Royer, A., Bostock, M., 2014. A comparative study of low frequency earthquake templates in northern Cascadia. Earth Planet. Sci. Lett. 402, 247–256.

Rubin, A.M., Armbruster, J.G., 2013. Imaging slow slip fronts in Cascadia with high precision cross-station tremor locations. Geochem. Geophys. Geosyst. 14, 5371–5392.

Schorlemmer, D., Gerstenberger, M., Wiemer, S., Jackson, D., Rhoades, D., 2007. Earthquake likelihood model testing. Seismol. Res. Lett. 78, 17–29.

Shelly, D.R., 2017. A 15-year catalog of more than 1 million low-frequency earthquakes: tracking tremor and slip along the deep san andreas fault. J. Geophys. Res., Solid Earth 122 (5), 3739–3753. http://dx.doi.org/10.1002/2017JB014047.

Shelly, D.R., Hardebeck, J.L., 2010. Precise tremor source locations and amplitude variations along the lower-crustal central San Andreas fault. Geophys. Res. Lett. 37.

Shelly, D.R., Beroza, G.C., Ide, S., Nakamula, S., 2006. Low-frequency earthquakes in Shikoku, Japan, and their relationship to episodic tremor and slip. Nature 442, 188–191.

Shelly, D.R., Peng, Z., Hill, D.P., Aiken, C., 2011. Triggered creep as a possible mechanism for delayed dynamic triggering of tremor and earthquakes. Nat. Geosci. 4, 384–388.

Trugman, D.T., Wu, C., Guyer, R.A., Johnson, P.A., 2015. Synchronous low frequency earthquakes and implications for deep San Andreas fault slip. Earth Planet. Sci. Lett. 424, 132–139.

Veen, A., Schoenberg, F.P., 2008. Estimation of space–time branching process models in seismology using an em–type algorithm. J. Am. Stat. Assoc. 103, 614–624.

Villegas-Lanza, J., Nocquet, J.-M., Rolandone, F., Vallée, M., Tavera, H., Bondoux, F., Tran, T., Martin, X., Chlieh, M., 2015. A mixed seismic-aseismic stress release episode in the Andean subduction zone. Nat. Geosci..

Wech, A.G., Creager, K.C., Houston, H., Vidale, J.E., 2010. An earthquake-like magnitude-frequency distribution of slow slip in northern Cascadia. Geophys. Res. Lett. 37.

Wesson, R.L., 1988. Dynamics of fault creep. J. Geophys. Res., Solid Earth 93, 8929–8951.

Wu, C., Guyer, R., Shelly, D., Trugman, D., Frank, W., Gomberg, J., Johnson, P., 2015. Spatial-temporal variation of low-frequency earthquake bursts near Parkfield, California. Geophys. J. Int. 202, 914–919.